IEEE Access
Multidisciplinary | Rapid Review | Open Access Journal

Received August 7, 2020, accepted August 29, 2020, date of publication September 18, 2020, date of current version October 1, 2020.

Digital Object Identifier 10.1109/ACCESS.2020.3024665

Disturbance Rejection Control Using a Novel Velocity Fusion Estimation Method for Levitation Control Systems

WENTAO XIA, ZHIQIANG LONG, AND FENGSHAN DOU
College of Intelligence Science and Technology, National University of Defense Technology, Changsha 410073, China

Corresponding author: Zhiqiang Long (zhqlong@nudt.edu.cn)

This work was supported by the 13th Five-year National Key Research and Development Program of China under Grant 2016YFB1200600.

ABSTRACT Magnetic levitation has been applied to maglev trains and magnetic suspension wind tunnel. However, there are some problems with the existing levitation control. For example, it is difficult to extract smooth velocity signals from the gap sensor with noise. The classical differentiator is susceptible to noise, which makes the levitation system sometimes vibrate. The accuracy and stability of levitation control need to be improved. The velocity fusion estimation method (VFE) is proposed to extract the velocity signal from the gap and acceleration sensor, which is theoretically derived to prove that it reduced the noise of the velocity signal. Then disturbance rejection control(DRC) is proposed that add VFE into classical levitation control. Because of the high-quality velocity signal and accelerometer's fast responsiveness, it makes DRC have many advantages. The advantages of using the proposed control structure are that it improved the control accuracy of the target gap and resisted disturbance effectively. Air-gap fluctuations in levitation systems can be reduced in transient pulse disturbance test, white noise disturbance test, and external force disturbance test when it applies the proposed control method. The effectiveness and advantages of the proposed control method are verified by the simulation and experiments.

INDEX TERMS Disturbance rejection, signal processing, levitation control, PID, differentiator.

I. INTRODUCTION

The Magnetic levitation is the process by which a ferromagnetic object is suspended in the air against gravity with the help of a magnetic field generated by a coil. This process presents many practical applications such as active magnetic bearings, vibration damping, suspension of wind tunnel models, transportation systems [1]. A magnetic levitation system, commonly composed of a coil, a levitating ball, and a vacuum space including sensors, makes up extremely nonlinear and unstable dynamics to control that suitable and reliable control method must be used. In the recent decade, numerous researches have been done on a laboratory scale in the field of position control of a magnetic levitation system [2]. An adaptive neural-fuzzy sliding mode controller (ANFSMC) is presented, which employs a sliding mode control, adaptive-fuzzy approximator, and the neural-fuzzy switching law. It reduces the impact of the disturbance and parameter perturbations with a smooth control current [3].

The associate editor coordinating the review of this manuscript and approving it for publication was Wei Xu.

A radial basis function (RBF) neural network modeling approach is introduced for the compensation of the non-contact inductive gap sensor of the high-speed maglev train. It can compensate for errors of the air gap sensor when the temperature changes from 20° to 80°C [4]. A radial basis function(RBF) neural network with functional weights (FWRBF) to approximate the coefficients of the state-dependent autoregressive model with exogenous input variables(SD-ARX), is built for modeling a magnetic levitation ball system and is referred to as the functional weight RBF nets-based ARX(FWRBF-ARX) model. It is suitable for controlling such an unstable, fast-response maglev system [5]. A robust nonlinear control strategy is developed for a class of second-order nonlinear uncertain systems with uncertainties and disturbances and is applied to two-axis active magnetic bearing position stabilization, It calculates and robustly cancels system uncertainties and disturbances via appropriate filtering [6]. A new criterion for selecting the weighting matrices of LQR is proposed, the experimental results prove that the proposed control strategy is effective in stabilizing the ball [7].

However, to the best of the author's knowledge, little attention was paid to the magnetic levitation continuous system and the ideal model. It is difficult to apply in engineering. so a simple, stable, reliable, and anti-jamming control method is needed in the engineering. In many cases, PID has proved itself to be an effective solution in control systems. It is easy to implement in engineering [1]. PID is the proportion, integral, and differential of error, and uses them to form feedback control states [8]. PI is often used only that has no error differential feedback because velocity signals are difficult to obtain in engineering [9]. Attraction type magnetic levitation devices are nonlinear and unstable systems with fast dynamics [10], so differential feedback control should be used in this system.

There are now two major engineering applications which are maglev train and magnetic levitation system that their air gap is relatively large.

The maglev train is a new type of urban rail transport. It has many advantages such as safety, low noise, environmentally, adaptability of line, minimal maintenance costs of construction, and ride comfort [11]. It was favored in many countries in recent years and the development prospects will be very broad. There are several commercial maglev lines built in China, Japan, and Korea. [12].

The magnetic levitation system is crucial to the maglev train. The magnetic levitation system is an unstable system, need to add feedback control to render it stable. But even with feedback control, magnetic levitation systems sometimes become unstable that it has noticeable vibrations. There are several reasons for this. For example, the flexible characteristics of the track [13] can cause vibration and instability of the levitation system in a maglev vehicle. Zhou Danfeng who is Chinese scholar has established a model of single point and single bogie levitation control system, linearised the model, obtained several different simplified block diagrams, analyzed the stability of the coupled system in the frequency domain, and proposed adaptive filter of the sensor signal to reduce the coupled vibration [14]. Liu Yaozong studied the dynamic response of single bogies under irregular electromagnetic force [15]. Li Jinhui designed a virtual energy harvester, which can reduce the coupled vibration [16]. The nonlinear nature of the system can also lead to vibration and instability of the levitation system because the characteristics of the system change accordingly in different levitation gaps and it makes the controller design even harder [17].

Another example is magnetic suspension wind tunnel balance [18].The magnetic suspension balance system [19], [20] benefits from its structure without physical supports, and the model being supported with levitation control system is an effective method to study the aerodynamic characteristics of the model, because the system can support the model without interfering with the test flow field, and can control the attitude of the model freely. Magnetic suspension balances use electromagnetic force to support models containing permanent magnets, so as to measure the aerodynamics of the aircraft without mechanical contact hanging in the wind tunnel [21], [22]. There is also vibration and instability in the magnetic suspension balance that is the same as the maglev train.

Vibration and instability of the levitation system can still occur which impact control precision [23]. Although the above-mentioned research and methods to reduce vibration, many control algorithms are prone to vibration and instability in the engineering practice of levitation control. This is because the impact of certain aspects of the real levitation system is ignored, such as the impact of chopper frequency and noise of gap sensors.

Moreover, most methods use velocity signals with unexpected noises and ignore the constraints of actuators' amplitudes, which may not be feasible in practical applications. A bounded output feedback controller without the need for velocity measurement is developed, which achieves accurate boom positioning and eliminates payload swings simultaneously. It was successfully applied to dual rotary crane systems. [24], but it hard to apply to magnetic levitation,because the targets are contactless in magnetic levitation and responsive which is unlike targets in dual rotary crane systems.

The classical differentiator can solve the problem that position signals haven't derivation when there are signal noise [25], [26], but it magnifies signal noise many times. Tracking differentials [27], [28] are used to extract velocity signals, it has a certain inhibitory effect on signal noise. But there are at least 4 parameters that need to be debugged and phase delay. If the parameters are not adjusted, the velocity curve is prone to oscillations or overturning. Another way is to gain velocity by integrating acceleration, which is the same as getting angular velocity by integrating the gyroscope [29].This method results in cumulative errors.

Many advanced and cutting-edge control theories cannot be widely used in practical engineering. One reason is that it is too complex, too many parameters that need to be debugged, and is prone to instability. Another reason is that there are always errors between theoretical models and actual physical objects, and some key factors may be overlooked.

To fundamentally solve this problem, sensor signal characteristics [30], [31] also need to be analyzed. There's a lot of disturbance in the actual engineering. [32], [33]. Next, this paper will explain how to bring the design of the levitation controller closer to the actual engineering. Then, the classical levitation control is modified, and a new control method is formed. The new control method inherits from the classical levitation control the quality that makes it the most widely used in engineering. Finally, the new control method is defined as DRC using VFE which has the good anti-jamming ability, which is to be verified with an experiment. In particular, the main contributions of this article lie in the following aspects.

1) The proposed VFE method deal with this problem that classical differentiator magnifies signal noise and the acceleration integrator drifts, which extracts less noise and a more realistic velocity.

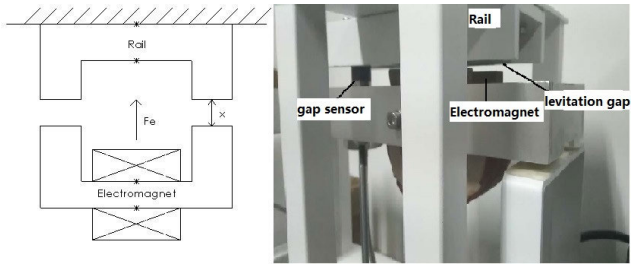

FIGURE 1. Simplified model of the levitation system in maglev train.

2) The proposed method in this paper has a higher ability to resist different disturbance than the classical levitation control. Disturbance includes pulse disturbance, white noise, and external force disturbance.

3) It has higher control accuracy and stability, such as sine tracking. The structure is simple and easy to apply because it only needs to be adjusted by one more parameter Q than the traditional suspension control.

This paper is organized as follows. In Section II, the subject of the study and the classical levitation control in this paper are described. In Section III, the problem exists in the levitation system has been introduced. In Section IV, it is theoretically derived the effect of noise signal on the classical levitation system. The VFE using multiple sensors is proposed for extracting high-quality velocity from the gap sensor and the accelerometer with noise. The advantage of the VFE is analyzed. In Section V, DRC using VFE is detailed and analyzed. In Section VI, experiment results are presented to show the effectiveness and advantages of the proposed control methods. In Section VI, the advantages and inadequacy of the methods and results were discussed and future work is given. Finally, the conclusions of this study are given in Section VII.

II. MODELING OF THE LEVITATION SYSTEM

Simplified model of the levitation system is shown in Fig.1. Single-iron levitation device consists mainly of an electromagnet and a fixed track. Enameled wire are wrapped around the U-shaped iron core to form an electromagnet. Electromagnetic iron coil through a certain current will produce a certain suction force on the fixed track. The distance between the upper surface of the electromagnet and the lower surface of the rail is a suspended gap, which is represented by x.

Electromagnetic iron produces electromagnetic force according to the air gap which is acquired by the gap sensor. The electromagnetic force can balance gravity and external disturbance by levitation control law [34]. The relationship between the air gap,the current, and the levitation force is:

$$Fe(i,x) = C_e \frac{i(t)^2}{x(t)^2} \tag{1}$$

where $F_e(i,x)$ is the electromagnetic force, $i(t)$ is the current through the electromagnet, the $x(t)$ is the air gap, C_e is the constant. [35]

$$C_e = \frac{\mu_0 N^2 A}{4} \tag{2}$$

where N is the number of turns of coil, μ_0 is the magnetic permeability of the vacuum, and A is the effective areas of the magnetic poles. the movement of electromagnet is:

$$m\frac{d^2x(t)}{d^2t} = mg - F_e(i,x) \tag{3}$$

where m is the quality of the electromagnet, the x displacement of the the electromagnet in the vertical direction,which is equivalent to the air gap. The relationship between the controlled current and voltage is:

$$\begin{aligned} U(t) &= \frac{d(L(t)i(t))}{dt} + Ri(t) \\ &= Ri(t) + \frac{\mu_0 N^2 A}{2x(t)}\frac{di(t)}{dt} + \frac{\mu_0 N^2 A i(t)}{2x^2(t)}\frac{dx(t)}{dt} \end{aligned} \tag{4}$$

where U is the voltage applied to the electromagnet.

Co-equation (1)-(4) gets Eq.(5)

$$\begin{cases} m\dfrac{d^2x(t)}{d^2t} = mg - C_e\dfrac{I(t)^2}{x(t)^2} \\ U(t) = Ri(t) + \dfrac{\mu_0 N^2 A}{2x(t)}\dfrac{di(t)}{dt} + \dfrac{\mu_0 N^2 A i(t)}{2x^2} \\ mg - F_e(i_0, x_0) = 0 \end{cases} \tag{5}$$

If the levitation system fluctuates near the equilibrium point, the inductor of the electromagnet can be considered a constant.

Eq.(4) can be reduced to Eq.(6)

$$U(t) = \frac{Ldi(t)}{dt} + Ri(t) \tag{6}$$

where $L = \frac{2C_e}{x_0}$.

Eq.(3) is deformed into Eq.(7) after linearization of work point.

$$m\frac{d^2x(t)}{d^2t} = \frac{2C_e i_0}{(x_0)^2}i - \frac{2C_e(i_0)^2}{(x_0)^3}x \tag{7}$$

x_1, x_2 and x_3 is state variables which are current, displacement and velocity.

$$\begin{cases} x_1 = i \\ x_2 = x \\ x_3 = \dot{x} \end{cases} \tag{8}$$

The linearized state equation of the levitation system can be obtained from Eq.(6),(7),(8).

$$\begin{cases} \dot{x_1} = \dfrac{-Rx_0}{2C_e}x_1 + \dfrac{x_0}{2C_e} \\ \dot{x_2} = x_3 \\ \dot{x_3} = \dfrac{2C_e i_0}{m(x_0)^2}x_1 - -\dfrac{2C_e(i_0)^2}{m(x_0)^3}x_2 \end{cases} \tag{9}$$

TABLE 1. Parameters of the levitation system in laboratory.

Physical parameter	value
Nominal air gap,x_0	0.004m
Inductance,L	0.12H
Electirc resistance of the magnet,R	5Ω
Mass of the magnet, m_e	2Kg
k_p	-5000
k_d	-100
k_I	-2000
k_i	10
x_0	0.004m

Eq.(9) is expressed as matrix vector form. The levitation gap value is output.

$$\begin{pmatrix} \dot{x_1} \\ \dot{x_2} \\ \dot{x_3} \end{pmatrix} = \begin{pmatrix} \frac{-Rx_0}{2C_e} & 0 & 0 \\ 0 & 0 & 1 \\ \frac{2C_e i_0}{m(x_0)^2} & -\frac{2C_e(i_0)^2}{m(x_0)^3} & 0 \end{pmatrix} \begin{pmatrix} x_1 \\ x_2 \\ x_3 \end{pmatrix} + \begin{pmatrix} \frac{x_0}{2C_e} \\ 0 \\ 0 \end{pmatrix} u_c \tag{10}$$

$$y = \begin{pmatrix} 0 & 1 & 0 \end{pmatrix} \begin{pmatrix} x_1 \\ x_2 \\ x_3 \end{pmatrix} \tag{11}$$

The voltage applied to the electromagnet, which adjust by current and position feedback control.

$$u_c = k_i\left(\frac{k_p(x - r_0) + k_d\frac{dx}{dt} + k_I\int_0^t (x - r_0)\,dt}{R} - i\right) \tag{12}$$

where x is the air gap. r_0 which is target of air gap. k_p, k_I, k_d are proportional, integral, differential control parameters of location feedback control. k_i is proportional feedback factor of current feedback.

The transfer function of output and input is Eq.(13), when it ignores the effect of integral feedback control on system stability

$$Y(S)/R(S) = \frac{\frac{2C_e i_0}{x_0^2}\frac{(k_p + k_d S)}{R}}{mS^2 - \frac{(2ki_0)k_d}{x^2 R}S - \frac{2ki_0 k_p}{x^2 R} - \frac{2k(i_0)^2}{x^3}} \tag{13}$$

The characteristic equation of linearization of the levitation system is Eq.(14).

$$mS^2 - \frac{(2C_e i_0)k_d}{x_0^2 R}S - \frac{(2C_e i_0 k_p}{(x_0^2 R)} - \frac{(2C_e(i_0)^2)}{x_0^3} = 0 \tag{14}$$

Value range for parameter k_p and k_d can be calculated by Routh's stability criterion. Such as $k_d < 0, kp < \frac{i_0 R}{x_0}$. Table 1 shows the parametric values of levitation system of single electromagnet in laboratory.

Linearizing the levitation system is mainly used to find out the range of control parameters. However, the system model is built to retain its nonlinearity which brings it closer to the real system. The classical levitation system control block diagram is presented in Fig.2.

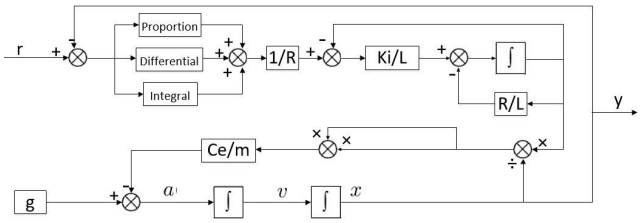

FIGURE 2. Block diagram of the classical control of the levitation system.

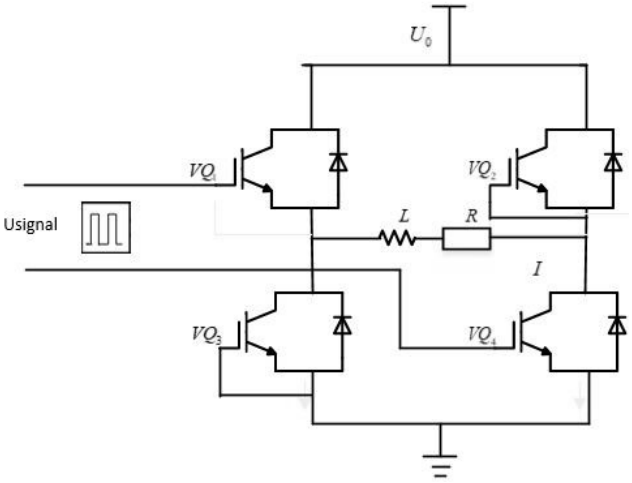

FIGURE 3. The chopper circuit schematic.

III. PROBLEM DESCRIPTION AND FORMULATION

A. EFFECT OF CHOPPER FREQUENCY ON LEVITATION SYSTEM PERFORMANCE

The control signal generated by the controller is low voltage PWM. The chopper converts Low voltage PWM signals are converted from choppers to high-voltage PWM signals which are applied to the coil of the electromagnet. The chopper is power devices. The chopper circuit schematic for the levitation system is shown in Fig.3. The chopper is an H-bridge structure made up of four power devices. The square wave control signal applied to VQ1 and VQ4, so it changes to the high-voltage PWM signal. U_0 is a supply voltage. L represents the electromagnet coil of the levitation system and R represents the resistance of the electromagnetic iron of the levitation system. The electromagnet generates an electric current due to the high-voltage PWM signal exerted on it, and the current on the electromagnet will have ripples.

As shown in Fig.4, the PWM signal of the current sensor and controller in the levitation system is collected that the frequency of the chopper is set to 1.4kHz and the sample rate is 10kHz. It can be analyzed from the figure when the PWM signal rises or falls, the current changes greatly.

Fig.5 is a simulation image of a PWM signal at different frequencies. Duty ratio for PWM signals is set to 50%. As observed in Fig.5, ripple at 1kHz signal is lower than that of the ripple at 500Hz signal, and ripple at 2kHz signal is less than that of the ripple at 1kHz signal. The higher the signal frequency, the smaller the ripple.

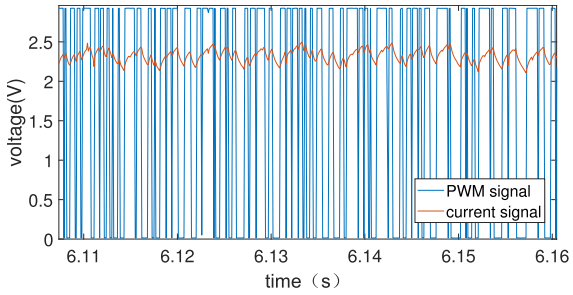

FIGURE 4. Current ripple curve and PWM signal.

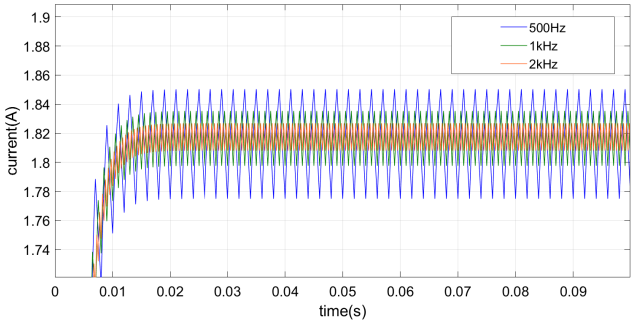

FIGURE 5. Electromagnetic iron current at different chopper frequencies.

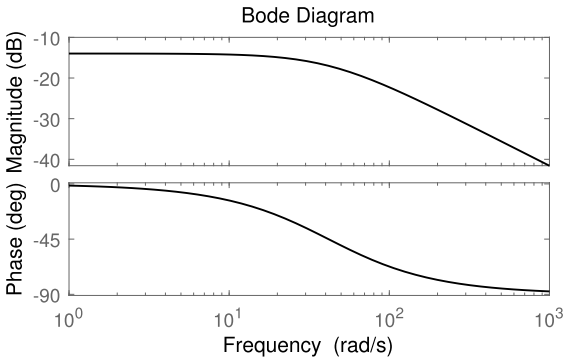

FIGURE 6. The bode diagram of transfer function between current and voltage.

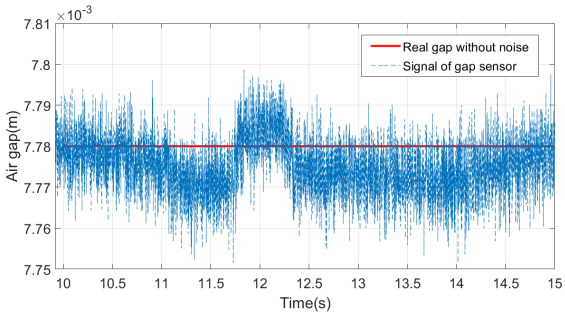

FIGURE 7. The signal of gap sensor and noise.

According to Eq.(15), the transfer function between I and U is:

$$\frac{I(S)}{U(S)} = \frac{1}{LS + R} \tag{15}$$

As is shown in Fig.6, the phase of the current lags behind the voltage. The higher the frequency of the voltage, the more the phase of the current lags behind the voltage. The higher the frequency of the voltage, the more the amplitude of the current decay. So the diagram can be explained why is the ripple of the higher signal frequency smaller. The ripple of the current affects the stability of the levitation system because the electromagnetic force on electromagnets is proportional to the square of the current. Theoretically, the higher the chopper frequency, the better the levitation stability, but that's not the case in practice. When the chopper frequency reaches a certain value, the levitation system is unstable, because the higher the chopper frequency, the more severe the electromagnetic disturbance. This disturbance affects the sensor signal.

B. EFFECT OF SIGNAL NOISE FROM THE GAP SENSOR ON THE LEVITATION SYSTEM

The noise of the gap sensor is the bandwidth band. It includes the disturbance of the chopper and the disturbance of the sensor itself. These disturbances can cause the signal to be unsmooth. For continuous systems, the derivative of the signal does not exist if the signal is not smooth or mutates, so PID control is difficult to implement. As being shown in the Eq.(16), the levitation control system is the discrete digital control in practice. Signal noise can cause the value of the differential to change very much, although the differential feedback includes the digital first-order low-pass filter.

$$C(Z) = k_p + k_I \cdot T_s \frac{1}{Z-1} + k_d \frac{N}{T_s + N \cdot T_s \frac{1}{Z-1}} \tag{16}$$

The red curve is a real gap without signal noise between 10 s and 15 s in Fig.7. The blue curve is the signal of the gap sensor with noise, and the value noise ranges from 7.76-7.8mm. Although the amplitude of white noise is not very large, the output of the controller Eq.(16) is very large. Because the differential in the Eq.(16) has the effect of amplifying the noise. Reasons are to be explored and a new method is to be proposed to overcome it in Part IV.

In order to analyze the distribution of noise energy from the levitation gap sensor across frequency domains, it can use Eq.(17) to get the power spectrum [36] of the gap sensor signal.

$$S_x(f) = \int_{-\infty}^{+\infty} G_x(\tau) e^{-j2\pi f \tau} d\tau \tag{17}$$

where $S_x(f)$ is autocorrelation function.

$$G_x(\tau) = x(f)x(t+\tau) \tag{18}$$

where τ is a time variable.

The gap sensor signal of the single-iron levitation device was gathered with the equipment that it's sampled at 3kHz. The power spectrum of the gap sensor signal is presented in the Fig.8. There're a lot of peaks and the most significant peak

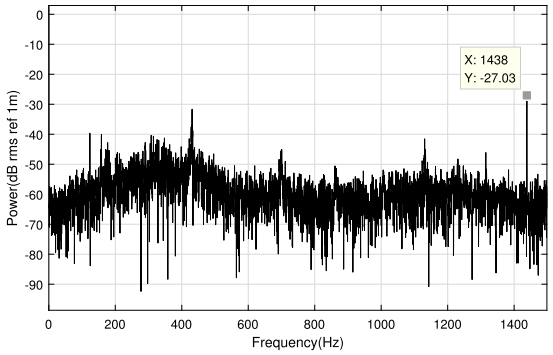

FIGURE 8. The power spectrum of gap sensor signal.

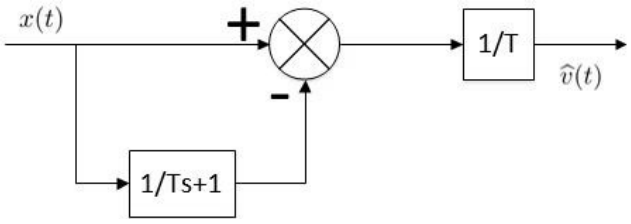

FIGURE 9. Block diagram of the classical differentiator.

is at 1438Hz, which is caused by electromagnetic conduction and radiation disturbance from choppers.

IV. THEORETICAL ANALYSIS OF VFE's ADVANTAGES

A. THE EXTRACTION METHOD OF THE VELOCITY SIGNAL IN THE TRADITIONAL LEVITAION CONTROL

In classical regulation theory, the differential signal is got by the Eq.(19) [27].As Fig.9 shows.

$$\widehat{v} = \omega(s)x = \frac{1}{T}(x - \frac{1}{Ts+1}x) \tag{19}$$

where x is the input of signal and y is the output of the signal of the classical differentiator. $\omega(s)$ is the transfer function of the classical differentiator. S is the Laplace variable. T is the time constant.

If the output of the $\frac{1}{Ts+1}$ is recorded as $\overline{x(t)}$, then Eq.(19) can be expressed as Eq.(20).

$$\widehat{v} = \omega(s)x = \frac{1}{T}(x(t) - \overline{x(t)}) \tag{20}$$

When the time constant is very small, Approximate equation for differentials is the following:

$$v(t) \approx \frac{x(t) - x(t-T)}{T} \tag{21}$$

where the delay signal $x(t-T)$ in the equation is achieved through inertial links $\frac{1}{Ts+1}$. The smaller the time constant is, the more accurate the differential signal is.

But if input signal $x(t)$ is contaminated by random noise $n_1(t)$, then Eq.(20) and Eq.(21) become the Eq.(22).

$$\widehat{v}(t) = \frac{1}{T}(x(t) + n_1(t) - \overline{x(t) + n_1(t)}) \tag{22}$$

where the delay signal $\overline{x(t) + n_1(t)}$ in the Eq.(22) is achieved through inertial links 1/(Ts+1) from $x(t) + n_1(t)$.

So it satisfies differential Eq.(23).

$$\frac{d\widehat{v}(t)}{dt} = -\frac{1}{T}(\widehat{v}(t) - (x(t) + n_1(t))) \tag{23}$$

If there is a solution to this equation, its expression is as following:

$$\begin{aligned}\widehat{v}(t) &= \int_0^{+\infty} e^{\frac{1}{T}(t-(\zeta))}(x(\zeta) + n_1(\zeta))d(\zeta) \\ &= \int_0^{+\infty} e^{\frac{1}{T}(t-\zeta)}(x(\zeta))d\zeta + \int_0^{+\infty} e^{\frac{1}{T}(t-\zeta)}(n_1(\zeta))d\zeta\end{aligned} \tag{24}$$

Since $n_1(\zeta)$ is a high-frequency noise that its mean value is zero, the integration is almost equal to zero, and the right-end integration is only the first item $\int_0^{+\infty} e^{\frac{1}{T}(t-\zeta)}(x(\zeta))d\zeta \approx v(t-T)$ remains. So Eq.(22) becomes Eq.(25).

The calculated velocity is equal to the real velocity plus the noise signal that is amplified 1/T times. Where T is time constant,which is less than 1.

$$\begin{aligned}\widehat{v}(t) &\approx \frac{1}{T}(x(t) + n_1(t) - x(t-T)) \\ &= \frac{1}{T}(x(t) - x(t-T) + n_1(t)) \\ &\approx \dot{x}(t) + \frac{1}{T}n_1(t)\end{aligned} \tag{25}$$

For acceleration, to obtain a velocity signal, acceleration needs to be integrated such as Eq.(26). Acceleration can also be noise and disturbance, that Eq.(26) becomes Eq.(27).

$$v(t) = \int_0^t a(t)dt \tag{26}$$

where a is acceleration, y is the output that it represents velocity in here.

As can be seen from the Eq.(27), the larger the integration item time t, the greater the error.

$$\begin{aligned}\widehat{v}(t) &= \int_0^t (a(t) + n_2(t))dt \\ &= \int_0^t (a(t))dt + \int_0^t (n_2(t))dt \\ &= v(t) + \int_0^t (n_2(t))dt\end{aligned} \tag{27}$$

where $a(t)$ is acceleration signal,$v(t)$ is a real velocity. $n_2(t)$ is the noise of the accelerometer. We can conclude that if the noise position signal is differential, the noise will be magnified 1/T times. If the acceleration signal is integrated, the error of the velocity signal increases over time.

B. VELOCITY FUSION ESTIMATION USE MULTI-SENSOR

Although the two methods do not seem very good, velocity is obtained by acceleration integral, which is accurate in a very short period of time, and velocity is obtained by differential signals of the gap sensor without cumulative error. In order

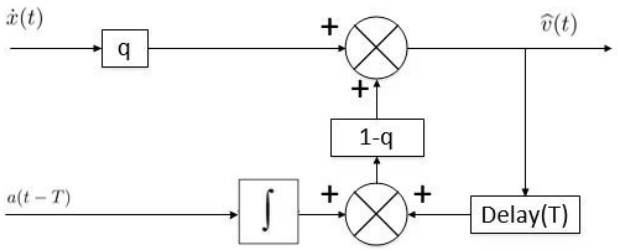

FIGURE 10. Block diagram of VFE algorithm.

to eliminate or reduce the noise amplification effect, it uses different types of sensors to make some kind of combination. The velocity signal is obtained by the fusion of the differential signal of the position signal. and the integral signal of acceleration. This method is VFE for velocity extraction which shows in Eq.(28). As Fig.10 shows.

$$\widehat{v}(t) = q(\dot{x}(t) + (1-q)(\widehat{v}(t-T) + a(t-T)T) \quad (28)$$

where q is the fusion factor. q range between 0.1 and 0.9. $\widehat{v}(t-T)$ is the output of the last time period.$\dot{x}$ is velocity obtained by the differential of the position signal at this moment. $a(t-T)$ is acceleration signal in the last time period.

Acceleration signal also has noise n_2. So Eq.(28) is as follows.

$$\begin{aligned}
\widehat{v}(t) &= q(\dot{x}(t) + \frac{1}{T}n_1(t)) + (1-q)(\widehat{v}(t-T) + a(t-T)T \\
&\quad + n_2(t)T) \\
&= q(\dot{x}(t)) + \frac{1}{T}(n_1(t)) + (1-q)(a(t-T)T) \\
&\quad + (1-q)n_2(t)T + (1-q)(q(\dot{x}(t-T) \\
&\quad + \frac{1}{T}n_1(t-T)) + (1-q)(\widehat{v}(t-2T) \\
&\quad + a(t-2T)T + n_2(t-T)T) \\
&= \dot{x}(t) + \frac{q}{T}n_1(t) + \frac{(1-q)q}{T}n_1(t-T) \\
&\quad + \frac{(1-q)^2 q}{T}n_1(t-2T) + \cdots + \frac{(1-q)^{\frac{t-T}{T}}q}{T}n_1(1) \\
&\quad + \frac{(1-q)^{\frac{t}{T}}q}{T}n_1(0) + (1-q)n_2(t-T)T \\
&\quad + (1-q)^2 n_2(t-2T)T + (1-q)^2 n_2(t-2T)T \\
&\quad + \cdots + (1-q)^{\frac{t-T}{T}}n_2(1)T + (1-q)^{\frac{t}{T}}n_2(0)T \\
&\approx \dot{x}(t) + \frac{q}{T}n_1(t) \quad \cdots (0.1 < q < 0.9)
\end{aligned} \quad (29)$$

where n_1 is noise of signal of the air gap, n_2 is noise of signal of acceleration. The means of n_1 and n_2 are close to zero. q and $(1-q)$is a positive number of less than 1, t is a time variable which is much greater than constant T, so $(1-q)^{\frac{t-T}{T}}$ and $(1-q)^{\frac{t}{T}}$ tends to be zero over time. The noise $n_2(t)$ is basically eliminated, because T is the control cycle which is 0.0005 which is small,and polynomials in Eq.(29) that contain $n_2(t)$ tend to be zero. The estimated velocity is approximately $\dot{x}(t) + \frac{q}{T}n_1(t)$, because some items in the equation can be ignored or offset against each other.

It can be concluded from Eq.(29)'s calculus that the velocity signal can be extracted by VFE, and the noise $\frac{1}{T}n_1(t)$ can be reduced compared to Eq.(25) because q is less than 1. This formula can be interpreted as follows. When the acceleration signal is integrated into the velocity, the longer the integration time, the cleaner the white noise filtering. However, there is a cumulative error when the integral interval is large. So the controller fuses the gap signal and the acceleration signal in each control cycle, which not only eliminates the cumulative error but also reduces the noise of the difference signal.

V. DISTURBANCE REJECTION CONTROL USING A VELOCITY FUSION ESTIMATION METHOD

A. CONTROL ALGORITHMS AND STRUCTURES

In engineering practice, sensor noise is inevitable. Velocity sought out by acceleration accumulation which is less affected by sensor noise, but the cumulative error will be severe, and the velocity of the result will drift seriously over time. How to get closer to real velocity from a noise gap sensor signal,that is a question resolved in Section IV. The VFE is applied to traditional controls and forms a new control structure, which is to suppress disturbance and improve control accuracy. Because there is a bias in the accelerometer, it needs to be remodeled before being applied. High-pass filtering can be added as Eq.(30) shows.

$$Filter(S) = \frac{bs}{bs+1} \quad (30)$$

where $b = \frac{1}{2\pi f_{cut}}$, f_{cut} is the cut-off frequency of the high-pass filter. Cut-off frequency for acceleration signals of levitation systems can be set to 0.5Hz.

In subsequent tests, continuous filters can not be applied in controller program unless they are transformed into discrete forms such as Eq.(31).

$$V_{out}(k) = h * V_{out}(k-1) + h * (V_{in}(k) - V_{in}(k-1)); \quad (31)$$

where $V_{in}(k-1)$ is the signal input from the previous moment. $V_{in}(k)$ is the signal input from this moment. $V_{out}(k-1)$ is the signal output from the previous moment. $V_{out}(k)$ is the signal output from this moment. H is a constant.

H can be calculated by Eq.(32). f_s is the sampling frequency of signal.

$$h = \frac{b}{b + \frac{1}{f_s}} \quad (32)$$

There is no cumulative error in the velocity at which the differentials are obtained using the gap sensor signal, so it can fuse signals of two different sensors. Velocity can be solved by Eq.(33).

$$\widehat{v}(k) = q\frac{x_2(k) - x_2(k-1)}{T_s} + (1-q)(\widehat{v}(k-1) + x_4(k-1)T_s) \quad (33)$$

where,$\widehat{v}(k)$ is the estimated velocity at now, $x_2(k)$ is the signal of the air gap sensor at now, $x_2(k-1)$ is the signal of the

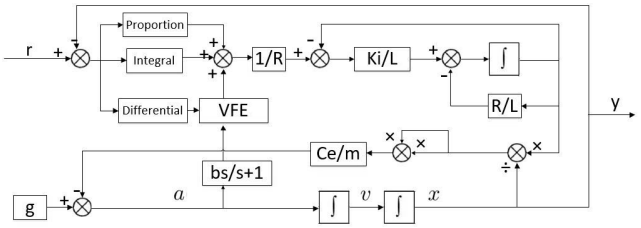

FIGURE 11. Block diagram of DRC using VFE.

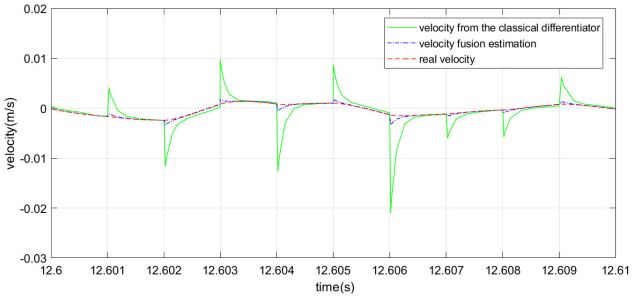

FIGURE 12. The velocity of elctromagnet under different algorithm.

air gap sensor at last time, $x_4(k-1)$ is acceleration value at last time, T_s is the time interval, q is a fusion coefficient. The control law of DRC is Eq.(34).

$$u_c = k_i\left(\frac{k_p(x-r_0)+k_d\widehat{v}+k_I\int_0^t (x-r_0)\,dt}{R} - i\right) \qquad (34)$$

In the new control strategy, the velocity used for differential feedback is estimated by the fusion of accelerometers and gap sensors. The Levitation system control block diagram changed from Fig.2 to Fig.11.

B. SIMULATION STUDY AND RESULTS

In this section, the control systems of Fig.2 and Fig.11 are calculated using numerical simulation with the parameters in Table 1. The q is 0.5. The initial air gap is given as 0.004m. Simulation step is 0.0005s. White noise is added into the gap sensor signal,that the magnitude is 0.0005m and sample time is 0.001s.

Velocity is obtained from gap differential signal and fusion estimation respectively. The red curve is the real velocity of the electromagnetic iron. The green curve is the gap differential signal which comes from noisy gap sensor. The blue curve is the velocity curve obtained by the velocity fusion estimation algorithm in this paper. The velocity fusion estimation algorithm uses a gap sensor and acceleration sensor to do complementary fusion filtering, the expression of which is shown in Eq.(33). We can draw conclusions from Fig.12, that there is a lot of noise in the gap differential signal, and the peak of the noise in the green curve is at least four times more than real velocity, while the value of velocity solved from both of acceleration sensor and gap sensor is closer to actual velocity.

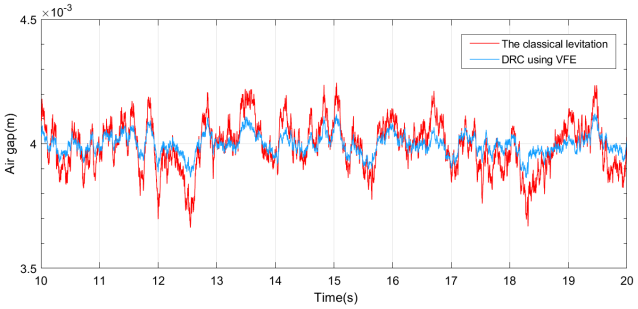

FIGURE 13. Comparison of levitation effects under different control strategies.

The gap signal is obtained from the simulation result of the levitation system shown in Fig.2 and Fig.11 respectively. As shown in Fig.13, the red curve varies between 3.66-4.25mm which uses the classical levitation controller expressed by Eq.(12). The blue curve is the air gap under the DRC using VFE method that the velocity of controller is from Eq.(33), and its value varies between 4.1-3.9mm. The new feedback control strategy reduces the vibration of the levitation system by about 2 times.

VI. EXPERIMENTAL VERIFICATION

In this section, the effectiveness of the designed controllers is demonstrated by the experiments. The experiments comprise the characteristics of the designed controllers, sine wave tracking performance,pulse disturbance tests and white noise disturbance tests, external force disturbance tests.

The experimental device consists of an experimental bench, levitation controller, chopper, and power supply. As shown in Fig.14, the experimental bench produces the corresponding electromagnetic force when there is current in the electromagnet coil. Current output by chopper which is controlled by the levitation controller. Levitation controller is powered by 5V, voltage for chopper is 36v. Voltage for gap sensor and accelerometer is $+-15$V. Sensitivity of the accelerometer is 1000 mV/g.The accelerometer is mounted on the electromagnet beam as shown in Fig.15.

The initial air gap is given as 0.004m. The control frequency is 2kHz and the frequency of the chopper is set to 1.4kHz. k_p is set as 2900, k_d is set as 55, k_I is set as 2880, q is set as 0.5.

To study the characteristics of the designed controllers in this paper, the gap signal, current signal and acceleration signal of the levitation system are collected, from the time of the experimental device power-up to 10s. As shown in Fig.16, this process is the levitation gap from 8mm to 4mm. The air gap at 8mm is the maximum, which represents the initial state before the power-up operation. The 4mm air gap is the target gap, which means that in the normal levitation state. It takes about 1s from the maximum gap to the target gap that is determined by the parameter k_I in the controller. The larger the k_I is, the shorter the time takes. What can it get from the current curve is that the current gradually increases at the beginning, then it gets the maximum. When the air

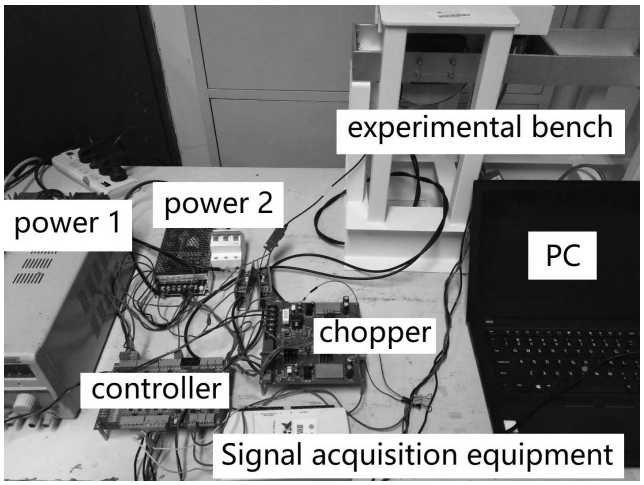

FIGURE 14. Laboratory and equipment.

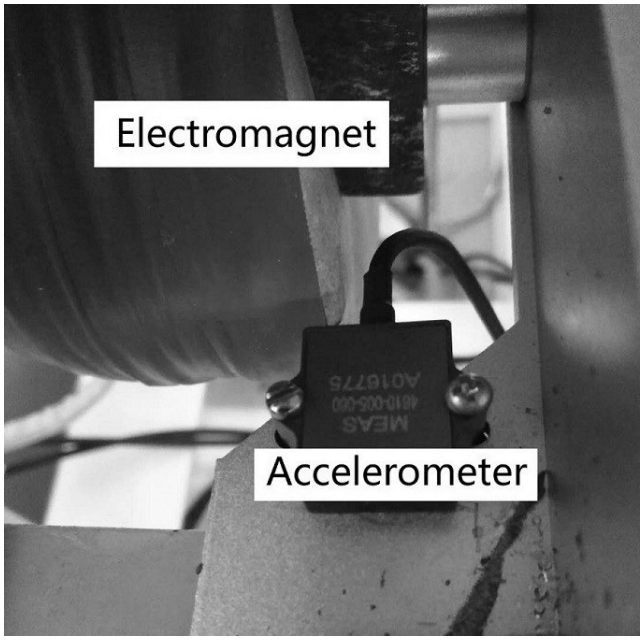

FIGURE 15. Location of the accelerometer installation.

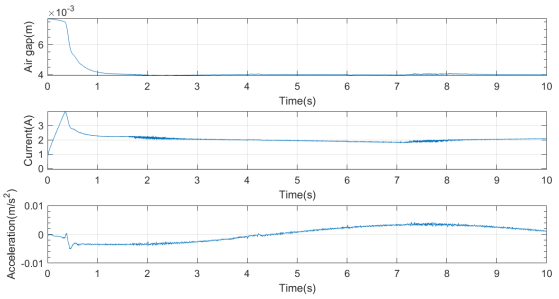

FIGURE 16. Test curve of levitation state of DRC usinng VFE.

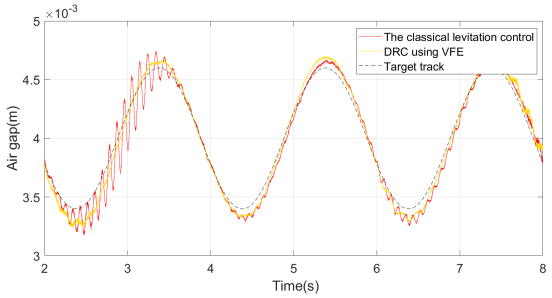

FIGURE 17. Comparison of sine wave tracking performance.

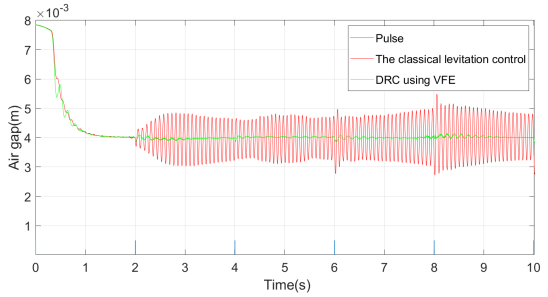

FIGURE 18. Comparison of pulse disturbance tests.

gap reaches the target, the current is 2A. The acceleration is relatively smooth throughout the levitation process, which means the system has almost no vibration.

It can be seen from Fig.17 that it is a comparison of sine wave tracking performance between traditional levitation control and the proposed control algorithm. Vibrations sometimes occur during the tracking process using the classical levitation control, while it's smooth using the proposed control algorithm. The proposed control strategy is superior to the existed classical levitation control strategy. The magnitude of the sine track is 0.5mm, the duration is 2 s.

In order to evaluate the superior disturbance rejection performance of the proposed method over the existing works, we have added comparison results between the proposed method in Fig.11 and the classical levitation control in Fig.2.

Firstly, pulse disturbance is added to the gap sensor signal. The magnitude of pulse disturbance is 0.5 mm, the duration is 2 s, and the pulse width is 0.5 ms. It can be seen from Fig. 18 that the maximum magnitude of fluctuation is less than 0.2mm in the green curve of DRC using VFE while curve of the classical levitation control vibrates in a magnitude of 2mm. The volatility of DRC at the pulse disturbance is about 10 times smaller than the classical levitation control.

Secondly, white noise disturbance is added to the gap sensor signal. The magnitude of white noise disturbance is 0.4 mm. It can be seen from Fig.19 that the curve of the classical levitation control vibrates in a magnitude of 2.4mm, and the maximum magnitude of fluctuation is less than 1mm in the green curve of DRC using VFE. The volatility of DRC at the equilibrium point is about 2 times smaller than the classical levitation control.

Thirdly, external force disturbance is added to the gap sensor signal. The magnitude of external force is 24.5 N and the direction is vertical down. It can be seen from Fig.20 that

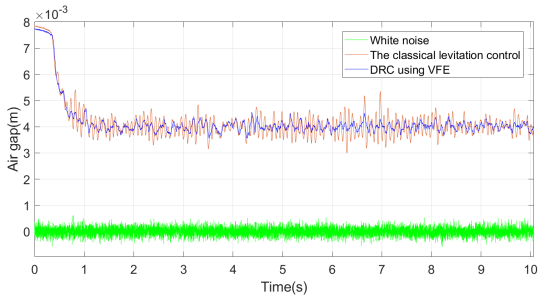

FIGURE 19. Comparison of white noise disturbance tests.

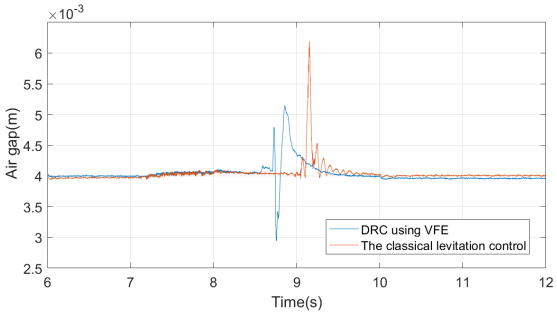

FIGURE 20. Comparison of external force disturbance tests.

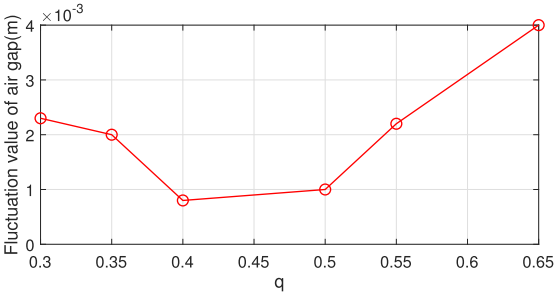

FIGURE 21. Disturbance rejection effect of different q on control system.

the air gap of the classical levitation control reaches 6.3mm, while the air gap of DRC using VFE reachs 5.1mm. Volatility peak of the proposed control method is 1.2mm smaller than the classical levitation control. This means the proposed control method responds more quickly than the classical control method.

VII. DISUSSION

Chopper frequencies and sensor noise affect the performance and stability of levitation systems. Properly raising the chopper frequency can reduce the vibration of the levitation system. But the chopping frequency shouldn't be too high. It interferes with the sensor signal and unstable the classical levitation system, which uses the classical differentiator. The noise of the chopper is caused by conduction and electromagnetic radiation disturbance, which is a narrow pulse disturbance signal. DRC solved this problem, which uses VEF to extract the velocity from the gap sensor and accelerometer. A lot of experiments were done which includes the test of the sine tracking, pulse disturbance, white noise, and external force disturbance. The results were analyzed. The results show that the proposed method in this paper has a higher ability to resist different disturbance than classical levitation control. Because the air gap of DRC fluctuates less, it has higher control accuracy and stability. It is not prone to collisions when there is great external interference,so it's safer and smoother.

In addition, there are some interesting questions that need further discussion. How to find the most suitable q(Fusion factor) and theoretically deduced it, that is a critical issue. The method of this article is to do many experiments to find suitable q. The effect of fusion factor q which is in Eq.(33) on the proposed levitation control system is shown in Fig.21. the floating amplitude of the air gap is small, and its performance of disturbance is good when q is 0.4 to 0.5. Beyond this range, the fluctuation increases, and the ability to resist white noise disturbance is weakened. The magnitude of white noise disturbance is 0.4 mm in the experiment of Fig.21.

However, why its performance of disturbance is good when q is 0.4 to 0.5, and how to to find and prove it in theory with a mathematical equation. The appropriate q range may be not the same for different control objects and disturbance. What's more, different sensor characteristics affect the appropriate q range. This is a difficult issue that we want to study further.

VIII. CONCLUSION

This paper studies a novel disturbance rejection control using a velocity fusion estimation method. The velocity fusion estimation method combines the advantages of position signals and acceleration signals. The proposed velocity fusion estimation method deals with the problem that classical differentiator magnifies signal noise and the acceleration integrator drifts, which extracts less noise and a more realistic velocity. It was revealed that the chopper and noise of gap sensors affect the performance of the levitation system. The proposed method is proved to be effective in resisting disturbance, its performance is better than the traditional levitation control method from the perspective of theoretical mathematical deduction, system simulation, and experiment.

REFERENCES

[1] A.-V. Duka, M. Dulău, and S.-E. Oltean, "IMC based PID control of a magnetic levitation system," *Procedia Technol.*, vol. 22, pp. 592–599, Jan. 2016.

[2] A. Fatemimoghadam, H. Toshani, and M. Manthouri, "Control of magnetic levitation system using recurrent neural network-based adaptive optimal backstepping strategy," *Trans. Inst. Meas. Control*, vol. 42, no. 13, pp. 2382–2395, Apr. 2020.

[3] Y. Sun, J. Xu, H. Qiang, and G. Lin, "Adaptive neural-fuzzy robust position control scheme for maglev train systems with experimental verification," *IEEE Trans. Ind. Electron.*, vol. 66, no. 11, pp. 8589–8599, Nov. 2019.

[4] Y. Jing, J. Xiao, and K. Zhang, "Compensation of gap sensor for high-speed maglev train with RBF neural network," *Trans. Inst. Meas. Control*, vol. 35, no. 7, pp. 933–939, Oct. 2013.

[5] Y. Qin, H. Peng, F. Zhou, X. Zeng, and J. Wu, "Nonlinear modeling and control approach to magnetic levitation ball system using functional weight RBF network-based state-dependent ARX model," *J. Franklin Inst.*, vol. 352, no. 10, pp. 4309–4338, Oct. 2015.

[6] A. Kuperman, "Uncertainty and disturbance estimator-assisted control of a two-axis active magnetic bearing," *Trans. Inst. Meas. Control*, vol. 38, no. 6, pp. 764–772, Jun. 2016.

[7] V. E. Kumar and J. Jerome, "LQR based optimal tuning of PID controller for trajectory tracking of magnetic levitation system," *Procedia Eng.*, vol. 64, pp. 254–264, Jan. 2013.
[8] J. Moreno-Valenzuela, R. Perez-Alcocer, M. Guerrero-Medina, and A. Dzul, "Nonlinear PID-type controller for quadrotor trajectory tracking," *IEEE/ASME Trans. Mechatronics*, vol. 23, no. 5, pp. 2436–2447, Oct. 2018.
[9] J. Moreno-Valenzuela and V. Santibáñez, "Robust saturated PI joint velocity control for robot manipulators," *Asian J. Control*, vol. 15, no. 1, pp. 64–79, Jan. 2013.
[10] C. I. Muresan, C. Ionescu, S. Folea, and R. De Keyser, "Fractional order control of unstable processes: The magnetic levitation study case," *Nonlinear Dyn.*, vol. 80, no. 4, pp. 1761–1772, Jun. 2015.
[11] Z. G. Sun, N. C. Cheung, S. W. Zhao, and W.-C. Gan, "Magnetic analysis of switched reluctance actuators in levitated linear transporters," *IEEE Trans. Veh. Technol.*, vol. 59, no. 9, pp. 4280–4288, Nov. 2010.
[12] X. Li, J. Geng, and D. Wang, "Dynamic responses of low–medium speed maglev train–simply supported beam interaction system," *Urban Rail Transit*, vol. 3, no. 3, pp. 136–141, Sep. 2017.
[13] Z. Wang, Y. Song, Z. Yin, R. Wang, and W. Zhang, "Random response analysis of axle-box bearing of a high-speed train excited by crosswinds and track irregularities," *IEEE Trans. Veh. Technol.*, vol. 68, no. 11, pp. 10607–10617, Nov. 2019.
[14] D. Zhou, P. Yu, L. Wang, and J. Li, "An adaptive vibration control method to suppress the vibration of the maglev train caused by track irregularities," *J. Sound Vib.*, vol. 408, pp. 331–350, Nov. 2017.
[15] Y. Liu, W. Deng, and P. Gong, "Dynamics of the bogie of maglev train with distributed magnetic forces," *Shock Vib.*, vol. 2015, Sep. 2015, Art. no. 896410.
[16] J. Li, J. Li, D. Zhou, P. Cui, L. Wang, and P. Yu, "The active control of maglev stationary self-excited vibration with a virtual energy harvester," *IEEE Trans. Ind. Electron.*, vol. 62, no. 5, pp. 2942–2951, May 2015.
[17] Y. Sun, J. Xu, H. Qiang, C. Chen, and G. Lin, "Adaptive sliding mode control of maglev system based on RBF neural network minimum parameter learning method," *Measurement*, vol. 141, pp. 217–226, Jul. 2019.
[18] E. E. Covert, M. Finston, M. Vlajinac, and T. Stephens, "Magnetic balance and suspension systems for use with wind tunnels," *Prog. Aerosp. Sci.*, vol. 14, pp. 27–107, Jan. 1973.
[19] D. Kai, H. Sugiura, and A. Tezuka, "Development of magnetic suspension and balance system for high-subsonic wind tunnel," *AIAA J.*, vol. 56, no. 7, pp. 8–12, 2018.
[20] Y. Takagi, H. Sawada, and S. Obayashi, "Development of magnetic suspension and balance system for intermittent supersonic wind tunnels," *AIAA J.*, vol. 54, no. 4, pp. 1277–1286, 2016.
[21] D.-K. Lee, J.-S. Lee, J.-H. Han, and Y. Kawamura, "Dynamic calibration of magnetic suspension and balance system for sting-free measurement in wind tunnel tests," *J. Mech. Sci. Technol.*, vol. 27, no. 7, pp. 1963–1970, Jul. 2013.
[22] H. Tanno, T. Komuro, K. Sato, K. Fujita, and S. J. Laurence, "Free-flight measurement technique in the free-piston high-enthalpy shock tunnel," *Rev. Sci. Instrum.*, vol. 85, no. 4, Apr. 2014, Art. no. 045112.
[23] M. Manetti, M. Morandini, and P. Mantegazza, "High precision massive shape control of magnetically levitated adaptive mirrors," *Control Eng. Pract.*, vol. 18, no. 12, pp. 1386–1398, Dec. 2010.
[24] N. Sun, Y. Fu, T. Yang, J. Zhang, Y. Fang, and X. Xin, "Nonlinear motion control of complicated dual rotary crane systems without velocity feedback: Design, analysis, and hardware experiments," *IEEE Trans. Autom. Sci. Eng.*, vol. 17, no. 2, pp. 1017–1029, Apr. 2020.
[25] W. Liu, J. Liu, Y. Gao, G. Wang, and Y.-L. Wang, "Multichannel signal detection in interference and noise when signal mismatch happens," *Signal Process.*, vol. 166, Jan. 2020, Art. no. 107268.
[26] J. Hebda-Sobkowicz, R. Zimroz, M. Pitera, and A. Wyłomańska, "Informative frequency band selection in the presence of non-Gaussian noise—A novel approach based on the conditional variance statistic with application to bearing fault diagnosis," *Mech. Syst. Signal Process.*, vol. 145, Nov. 2020, Art. no. 106971.
[27] J. Han, "From PID to active disturbance rejection control," *IEEE Trans. Ind. Electron.*, vol. 56, no. 3, pp. 900–906, Mar. 2009.
[28] R. Patelski and P. Dutkiewicz, "On the stability of ADRC for manipulators with modelling uncertainties," *ISA Trans.*, vol. 102, pp. 295–303, Jul. 2020.
[29] H. He, B. Zhu, and F. Zha, "Particle swarm optimization-based gyro drift estimation method for inertial navigation system," *IEEE Access*, vol. 7, pp. 55788–55796, 2019.
[30] X. Yu, G. Jin, and J. Li, "Target tracking algorithm for system with Gaussian/non-Gaussian multiplicative noise," *IEEE Trans. Veh. Technol.*, vol. 69, no. 1, pp. 90–100, Jan. 2020.
[31] W. Wei, W. Xue, and D. Li, "On disturbance rejection in magnetic levitation," *Control Eng. Pract.*, vol. 82, pp. 24–35, Jan. 2019.
[32] K. Jerath, S. Brennan, and C. Lagoa, "Bridging the gap between sensor noise modeling and sensor characterization," *Measurement*, vol. 116, pp. 350–366, Feb. 2018.
[33] S.-H. Park, S.-H. Lee, S.-H. Park, Y.-H. Sohn, Y. Huh, G.-H. Cho, and C.-T. Rim, "Precise and robust Hall effect gap sensor with common electrical and magnetic noise reduction technique," in *Proc. Int. Conf. Electron Devices Solid-State Circuits (EDSSC)*, Oct. 2017, pp. 1–2.
[34] H. S. Han, B. H. Yim, N. J. Lee, Y. C. Hur, and S. S. Kim, "Effects of the guideway's vibrational characteristics on the dynamics of a maglev vehicle," *Vehicle Syst. Dyn.*, vol. 47, no. 3, pp. 309–324, Mar. 2009.
[35] H.-S. Han and D.-S. Kim, *Magnetic Levitation: Maglev Technology and Applications*. Dordrecht, The Netherlands: Springer, 2018.
[36] E. Vallarino, S. Sommariva, M. Piana, and A. Sorrentino, "On the two-step estimation of the cross-power spectrum for dynamical linear inverse problems," *Inverse Problems*, vol. 36, no. 4, Apr. 2020, Art. no. 045010.

WENTAO XIA was born in 1993. He received the B.S. degree in mechanical and control engineering, in 2015, and the M.S. degree in mechanical and electronic engineering from Dalian University, Dalian, China, in 2018. He is currently pursuing the Ph.D. degree with the College of Intelligence Science and Technology, National University of Defense Technology, Changsha, China. His current interests include control science and engineering. His research interests include levitation control technology and coupling vibrations.

ZHIQIANG LONG received the B.S. degree in automation from the Huazhong University of Science and Technology, Wuhan, China, in 1988, the M.S. degree in flight mechanics from the Harbin Institute of Technology, Harbin, China, in 1991, and the Ph.D. degree in control science and engineering from the National University of Defense Technology, Changsha, China, in 2010. He is currently working as a Professor with the National University of Defense Technology. He is also the Head Research Engineer with the Engineering Research Center of Maglev Technology. His research interests include magnetic levitation control, fault diagnosis, tolerant control for maglev trains, and new maglev technology.

FENGSHAN DOU was born in Shandong, China, in 1977. He received the M.S. degree in control science and engineering from the National University of Defense Technology, Changsha, China, in 2007. He is currently working as an Associate Professor with the Engineering Research Center of Maglev Technology, National University of Defense Technology. His research interests include fault diagnosis, detection technology, and new maglev technology.